Electronic Supplementary Material (ESI) for Energy & Environmental Science.

Electronic Supplementary Information:

Green ethylene production in the UK by 2035: A techno-economic assessment

Andreas H. Nyhus[a,1], Maria Yliruka[a,1.]*, Nilay Shah[a], and Benoît Chachuat[a,]*

Table of Contents

S. 1 Thermocatalytic Process Modelling 5
S. 1.1 Methanol Synthesis (MS) 5
S. 1.2 Methanol to Olefins (MTO) 6
S. 1.3 CO_2 Methanation (CTM) 9
S. 1.4 Oxidative Coupling of Methane (OCM) 11
S. 1.5 Syngas Fischer-Tropsch Synthesis (S-FT) 12
S. 1.6 Direct Fischer-Tropsch Synthesis (D-FT) 14
S. 2 Electrocatalytic Processes 16
S. 2.1 Process Modelling 16
S. 2.1.1 Low-Temperature Electrocatalytic Processes 16
S. 2.1.2 High-Temperature Electrocatalytic Processes 21
S. 2.2 Electrocatalytic Processes including Product Separation 22
S. 2.2.1 CO_2 Electroreduction to Methane (eCH_4) 22
S. 2.2.2 Direct CO_2 Electroreduction to Ethylene (D-eC_2H_4) 23
S. 2.2.3 CO Electroreduction to Ethylene (S-eC_2H_4) 24
S. 2.2.4 CO_2 Electroreduction to Carbon Monoxide (eCO) 25
S. 2.2.5 Exclusion of Liquid Product from eCH_4 and S-eC_2H_4 processes 25
S. 2.2.6 Fixed Capital Investment of the Low-Temperature Electrocatalytic Processes . 26
S. 3 Olefin Production in the UK 27
S. 4 Economic Allocation Factor versus Cash Flow Analysis 27
S. 5 Techno-Economic Assessment 28
S. 6 Detailed Energy and Mass Balances 29
S. 6.1 MS + MTO 29
S. 6.2 CTM + OCM 30
S. 6.3 eCH_4 + OCM 31
S. 6.4 eCO + S-FT 32
S. 6.5 eCO + S-eC_2H_4 33
S. 6.6 HTeCO + S-FT 34
S. 6.7 HTeCO + S-eC_2H_4 35
S. 6.8 D-FT 36
S. 6.9 D-eC_2H_4 37
References 38

Structure

The document is structured in six parts: In Section S.1, the adaptions of the references for the thermocatalytic processes to the new system boundary for green ethylene production are explained. Section S.2 presents the general set of equations underlying the electrocatalytic process models developed herein. Additionally, Section S.2 provides a process block diagram for each of the electrocatalytic processes including their respective separation processes. Section S.3 characterises the olefins production plants in the United Kingdom. Section S.4 shows that the economic allocation factor in our work is aligned with the commonly used cash flow method. Section S.5 complements Section 2.2. of the publication by providing more detail on the economic parameters of the techno-economic assessment. Finally, Section S.6 presents detailed energy and mass balances for the integrated stage-1 and stage-2 processes shown in Fig.2 of the publication.

Abbreviations and mathematical notation

C	Compressor
MS	Methanol synthesis
MSR	Methanol Synthesis Reactor
FS	Flash Separation
DC	Distillation Column
P	Pump
MTO	Methanol to Olefins
MTOR	Methanol-to-Olefins Reactor
Q	Quench
CTM	CO_2 Methanation
CTMR	Carbon-to-Methane Reactor
ASU	Air Separation Unit
OCM	Oxidative coupling of methane
OCMR	Oxidative Coupling of Methane Reactor
CC	Carbon Capture
Met	Methanator
FU	Furnace
S-FT	Syngas Fischer-Tropsch
SFTR	Syngas Fischer-Tropsch Reactor
EtVPSA	Vacuum Pressure Swing Adsorption for Ethylene-separation
D-FT	Direct Fischer-Tropsch
DFTR	Direct Fischer-Tropsch Reactor
Mem	Membrane
CHP	Combined Heat and Power Unit
RWGS	Reverse water gas shift
HEX-INT	Heat exchanger for heat integration

HEX-HH	Heat exchanger for high heat
HPS	High-Pressure Steam
HEX	Heat Exchanger
PSA	Pressure Swing Adsorption
OER	Oxygen Evolution Reaction
RHE	Reversible Hydrogen Electrode
SCE	Saturated Calomel Electrode
HER	Hydrogen Evolution Reaction
CCM	Catalyst-Coated Membrane
BOP	Balance of Plant
AEM	Alkaline Exchange Membrane
PEM	Proton Exchange Membrane
VPSA	Vacuum Pressure Swing Adsorption
EL	Electrolyser
ABS	Absorption Column
E-DC	Extractive Distillation Column
TIC	Total Investment Cost
OSBL	Outside Battery Limit
ABS	Absorption Column
E-DC	Extractive Distillation Column
EL	Electrolyser
CapEx	Capital Expenditure
$Cost_{turb}$	Cost of turbine
P_turb	Power of turbine
$Cost_{HEX}$	Cost of heat exchanger
A_{HEX}	Heat transfer area of heat exchanger
$Cost_{pump}$	Cost of pump
$\dot{V}$	Volumetric flow rate through pump
$Cost_r$	Capital cost of process unit r
S_0	Base capacity of process unit r
S_r	Capacity of process unit r
$Cost_0$	Base capital cost of process unit r
s_f	Scaling factor
E_r	Energy consumption by process unit r
E_0	Base energy consumption or process unit r
$\eta_{F,i}$	Faradaic efficiency of component i
j	Current density
E_{red}^{SHE}	Half-cell electrode potential
$\dot{n}_{C_2H_4}$	Molar flow rate of ethylene
F	Faraday constant

I	Current
z_i	Number of electrons transferred
$\dot{n}_i$	Molar flow rate of component i
$\dot{n}_{CO_2}^{st}$	Stoichiometric molar flow rate of CO_2
X_{CO}	Conversion of CO_2
ΔE_{op}	Overpotential
$E_{red,OER}^{0}$	Standard reduction potential of the oxygen evolution reaction
A_{cell}	Electrode area
$Cost_{ccm}$	Cost of catalyst-coated membrane
f_{ccm}	Fraction of CCM cost of future PEM electrolysers
$f_{HT,stack}$	Fraction of the stack cost on the system cost for HT CO electrolyser
$SC_{HT,ref}$	Specific cost of HT CO electrolysers
$Cost_{stack,LT}$	Capital cost of the stack in LT CO_2/CO electrolysers
$Cost_{stack,HT}$	Capital cost of the stack in HT CO electrolyser
$Cost_{system,LT}$	Total system cost of LT CO_2/CO electrolyser
$Cost_{system,HT}$	Total system cost of HT CO electrolyser
$SC_{BOP,LT}$	Specific cost of the balance of plant of LT CO_2/CO electrolysers
LT	Lifetime
s	Stack replacements
f_{UF}	Utilisation factor
P	Electrolyser power consumption
r	Interest rate
f_{er}	Cost fraction of plant erection
f_c	Cost fraction of civil engineering
f_{sb}	Cost fraction of structures and buildings
FCI	Fixed capital investment
$Cost_{FCI,EL}$	Total fixed capital investment of electrolyser
MA	Mixed amine
C_0	Capital cost of separation process in electrocatalytic processes
n	Economies of scale scaling factor
$Cost_{FCI,sp}$	FCI of separation process
f_{IC}	Cost fraction of piping, engineering and construction
$Cost_{FCI,tot}$	Total FCI of electrocatalytic process
$Cost_{wc}$	Working capital
$Cost_{start}$	Cost of start-up
$Cost_{cont}$	Cost of contingencies
$t_{20\%}$	Time to achieve 20% concentration of liquid product in electrolyte
$LCOEt$	Levelised cost of ethylene
$OpEx$	Operating expenditure
CRF	Cost reduction factor

m_e	Production rate of ethylene
$Cost_j$	Price of side-product j
m_j	Production rate of side-product j
AF_{econ}	Economic allocation factor

S. 1 Thermocatalytic Process Modelling

In the following, the process flowsheet as provided in the reference is presented in form of a process block diagram. Where applicable, modifications made to the reference processes are detailed. For simplicity, it is assumed that any impurities in the recycle stream or the intermediate stream after separation can be neglected. Where multiple heat integrated process designs are available in the reference, the cheapest process is chosen. Where a net import of hot utility is required, the system is extended to include a hydrogen boiler which is assimilated to a condensing steam boiler with an efficiency of 89% and specific capital costs of 43 £/kW as presented in Olympios et al. (1).

S. 1.1 Methanol Synthesis (MS)

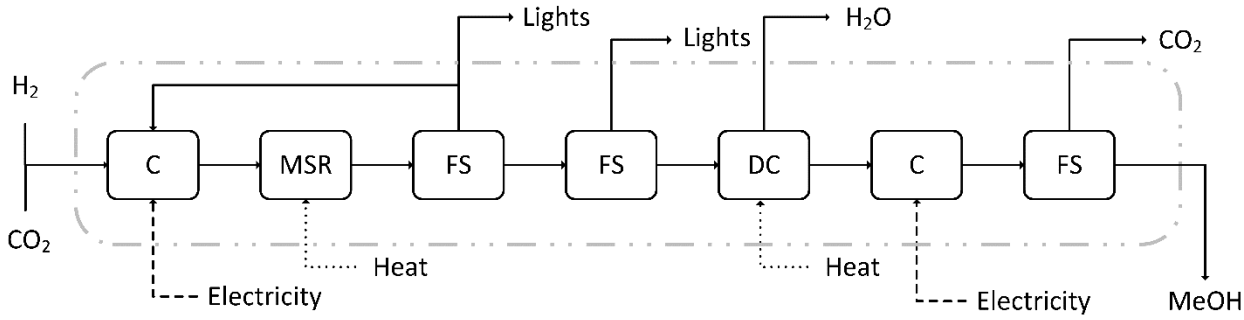

Figure S. 1: In the methanol synthesis from CO_2 and hydrogen as modelled by Perez-Fortes et al. (2)*, both inlet streams are first compressed to 78 bar (C) before entering the adiabatic plug flow reactor (MSR) to be converted to methanol. Unconverted H_2 and carbon oxides are separated from the liquid phase in a flash vessel (FS) and recycled to the reactor with 1% of the recycle stream being purged. Using a second FS, an almost gas-free mixture of methanol and water is obtained (63 wt%$_{MeOH}$). The mixture is fed to a distillation column (DC) to recover methanol at the top. The methanol stream is compressed (C) before it is condensed (FS) and any remaining inert gases being purged. The final methanol stream has a purity of > 99.9 wt%.*

The reference for the MS process as described in Perez-Fortes et al. (2) remained unchanged and is summarised in Figure S.1.

S. 1.2 Methanol to Olefins (MTO)

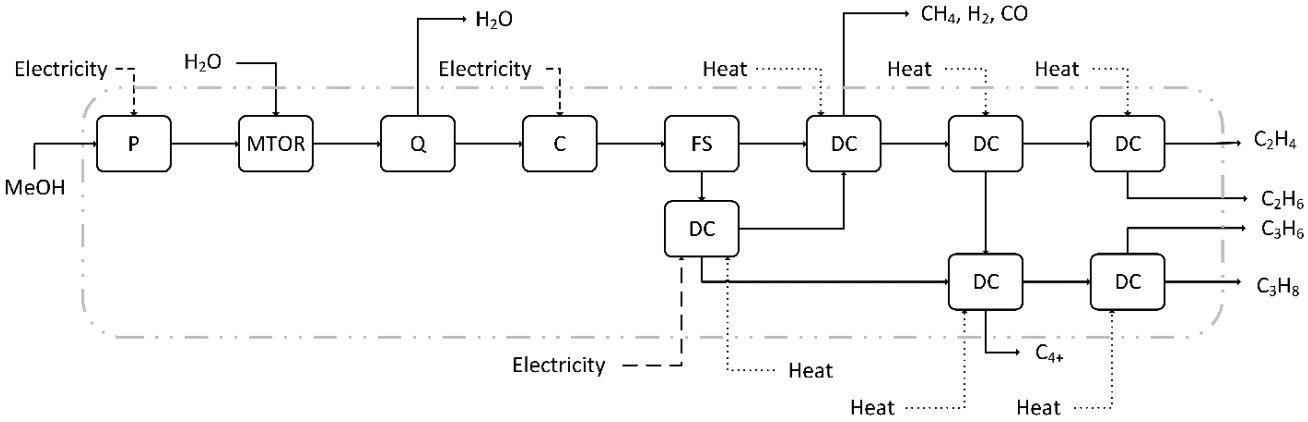

Figure S. 2: The methanol stream is preheated to 150 °C (P) and together with steam fed to the fluidized bed reactor (400°C, 3 bar) (MTOR). The product stream is quenched (Q) and impurities are removed in the discharged water. The vapor stream is compressed (C) and then split into vapor and organic liquid phase in a flash vessel (FS). The light components are removed from the vapor, before sending it to the demethanizer (DC). A condensate splitter (DC) is used to recover the C3+ products from the liquid phase and sent it to the depropanizer. The bottom product of the demethanizer enters a deethanizer (DC) and followed by a C_2-splitter (DC) to recover ethylene and ethane from the top product. The bottom product of the deethanizer feeds into the depropanizer (DC) of which the top product goes to a C_3-splitter (DC) to recover propylene and propane. Ethylene and propylene are both produced at polymer grade (99.5 wt%).

The MTO process as presented in Chen et al. (3) had to be modified in two ways. Firstly, the mass balance around the water removal units (D-101, D-102) and the CO_2 removal unit (A-101) in the conditioning section of the original flowsheet were stated incorrectly and therefore the streams were recalculated. The updated flow rates and compositions are provided in Table S. 1.

Table S. 1: The stream table presents updated flow rates and compositions for parts of the process flowsheet presented Chen et al. (3)*. The streams represent waste water (Stream 29), condensate from the splitter (Stream 31) and captured CO_2 (Stream 30).*

Process unit (original)	**D-101**	**A-101 & D-102**	**T-204**
Stream	29	30	31
Temperature (℃)			9.8
Pressure (bar)			27
Vapor frac			1
Mole Flow (kmol/hr)	16.0	99.7	225.64
Mass Flow (kg/hr)	317.3	4127.8	6587.20
Molar composition (%)			
H_2	4.9	0.7	0.3
CO	3.9	0.9	0.3
CH_4	0.0	0.0	3.4
C_2H_4	0.0	1.1	83
C_2H_6	0.0	1.3	2.2
CO_2	0.0	86.0	3.7
C_3H_6	0.0	0.4	7.1
C_3H_8	0.0	1.0	trace
C_4H_8	0.0	0.0	0
C_4H_{10}	0.0	0.9	0
C_5H_{10}	0.0	0.0	0
C_6H_{12}	0.0	0.0	0
CH_3OH	16.2	0.6	0
H_2O	75.0	7.1	0

Secondly, Chen et al. (4) did not account for the energy required to produce the steam needed to heat the reactor. However, the reference indicates that excess heat from the reactor is available: *"MTO process releases significant amount of reaction heat, which can be utilized by generating high pressure steam (HPS)"*. To comply with the methodology described in Section 2.2.1 of the main manuscript, a heat integration loop was explicitly designed and is shown in Figure S. 3. The energy balance is calculated by selecting temperature, pressure and state of each stream based on the steam tables in Green et al. (16).

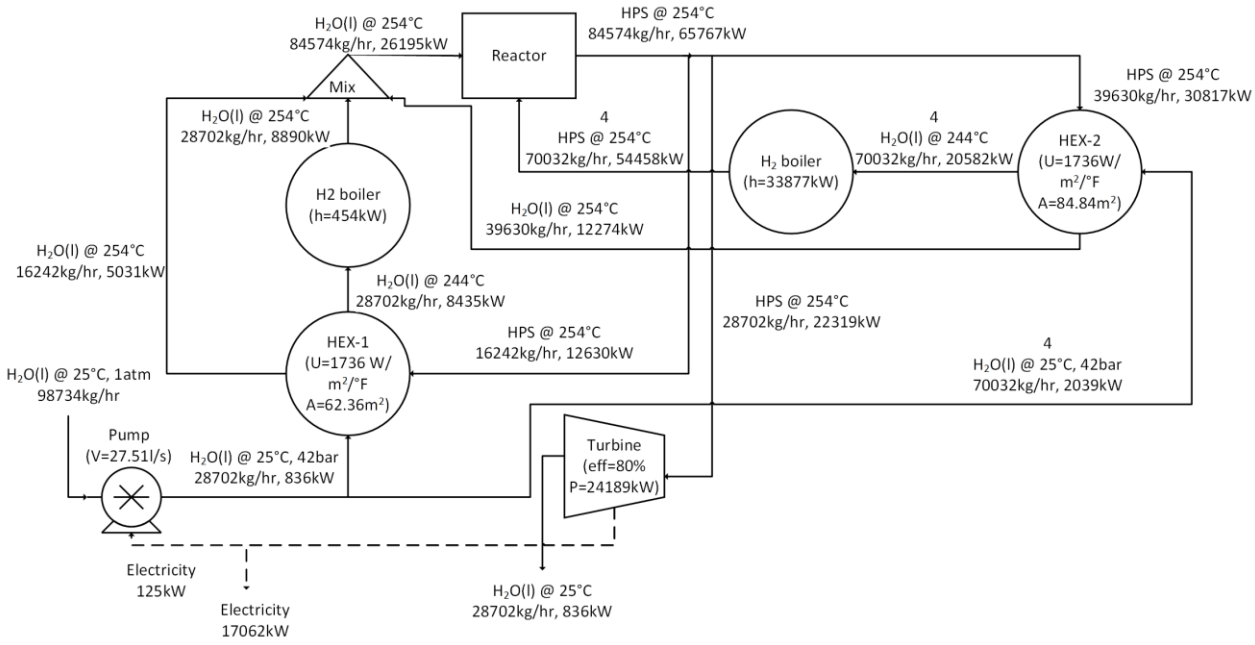

Figure S. 3: The system of heat exchangers and hydrogen boilers was explicitly designed to integrate the excess heat of the reactor to create the high-pressure steam that is fed as a reactant to the reactor. Stream 4 was defined according to the flowsheet presented in Chen et al. (4).

The capital expenditure of the steam turbine, heat exchangers and pump were based on cost correlations presented in Towler and Sinnot (5), converting USD2010 using a CEPCI of 523.9 and an exchange rate of 1.26 USD/GBP (6). The capital expenditure (CapEx) of the steam turbine ($Cost_{Turb}$) in Figure S.3 can be estimated based on its power consumption (P_{Turb}) by Eq. 1.

$$Cost_{Turb} = -14{,}000 + 1{,}900 \cdot {P_{Turb}}^{0.75} \qquad \text{(Eq. 1)}$$

A counter-current flow through the heat exchanger (HEX) and an overall heat transfer coefficient of 550 btu hr^{-1} ft^{-2} (5) were assumed. Hence, the capital cost of the HEX ($Cost_{HEX}$) was determined based on its heat transfer area (A_{HEX} in [m^2]) by Eq. 2.

$$Cost_{HEX} = 28{,}000 + 54 \cdot A_{HEX}^{1.2} \qquad \text{(Eq. 2)}$$

Finally, the capital cost of the water pump ($Cost_{Pump}$) were derived based on the volumetric flow rate ($\dot{V}$ in [L s^{-1}]) according to Eq. 3.

$$Cost_{Pump} = 8{,}000 + 240 \cdot \dot{V}^{0.9} \qquad \text{(Eq. 3)}$$

Table S. 2: The capital cost for the steam cycle shown in Fig. S.3 are summarised.

Equipment	**Capital cost [k£2019]**
Steam turbine	4260
Heat exchanger (HEX-1)	37
Heat exchanger (HEX-2)	45
Water pump	14
H2 Boiler-1	1460
H2 Boiler-2	19

S. 1.3 CO_2 Methanation (CTM)

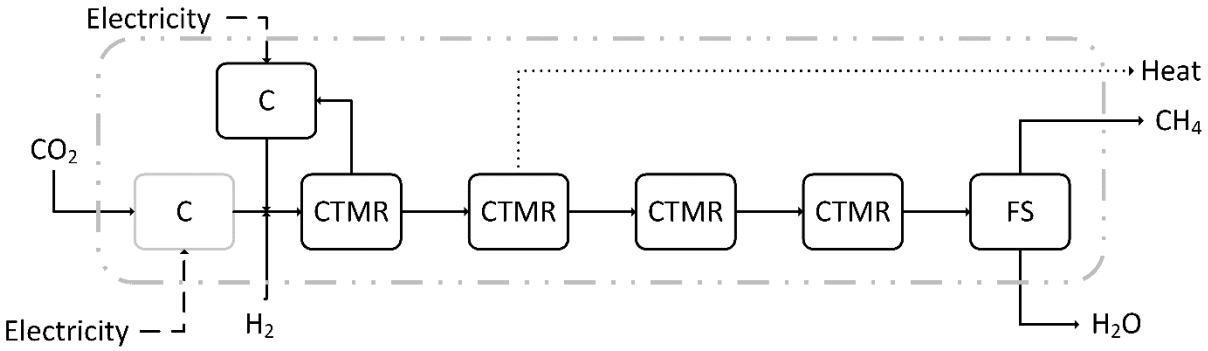

Figure S. 4: For the CO_2 methanation, a series of four adiabatic fixed bed reactors (CTMR) are used to avoid cooking and sintering of the catalyst. The synthetic natural gas is subsequently cooled and dried in a flash unit (FS).

While the CO_2 capture and compression units were excluded from the original flowsheet provided in (7), the methanation process itself remained unchanged. The process block diagram had to be extended by a compression stage to match the pressure of feed stream to the OCM process, that represents the stage-2 process converting methane to ethylene. A two-stage compressor was explicitly designed in Aspen Plus V.11 to increase the pressure of the outlet stream from 9 bar to the 70 bar as shown in Figure S. 5. The electricity demand of the compressor is 74 kW and its capital cost are 1.2 M£.

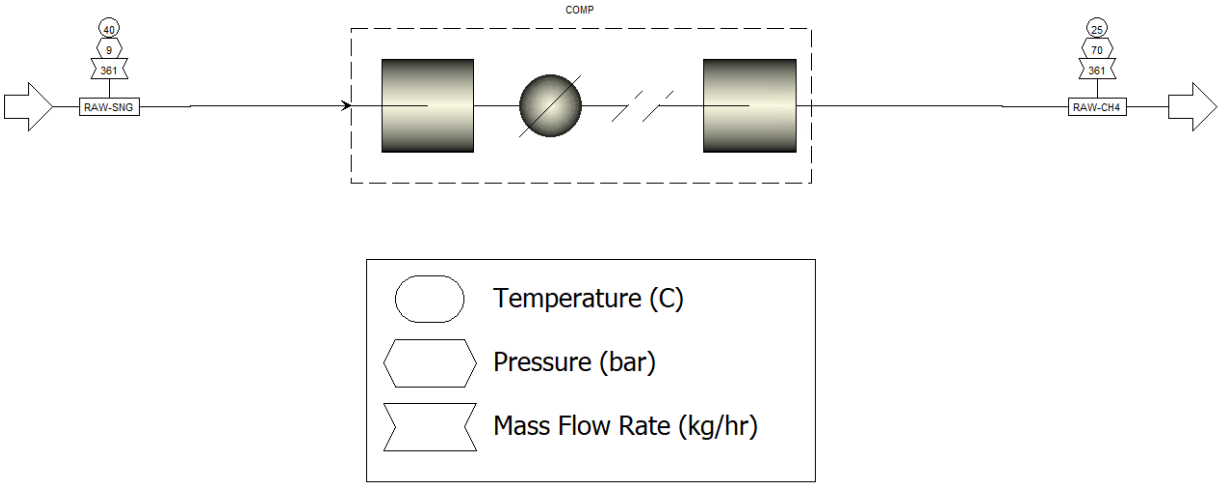

Figure S. 5: A schematic of the two-stage compressor for the CTM process and the characteristics of the inlet and outlet streams are shown.

As the carbon capture unit is excluded from the flowsheet in Chauvy et al. (7), the heat released from the catalytic methanation becomes available as it is no longer used in the reboiler of the capture unit or the stripping column. Therefore, a condensing steam turbine is designed to convert the excess heat in 185 °C, 8 bar steam to electricity. The capital cost of the steam turbine is calculated as outlined in section S. 2.1. Even after meeting the electricity demand of the compression unit and the OCM process, an electricity surplus is available as summarised in Table S. 3.

Table S. 3: Overview about the electricity produced and consumed in the CTM process, as well as the excess electricity that can be integrated with the subsequent oxidative coupling of methane.

Available excess heat from methanation reactors, [kW]	931.62
Electricity produced from excess heat with $\eta_{Turb} = 0.8$, [kW]	745.30
Electricity consumed for the compression of methane, [kW]	74.08
Electricity available for integration with stage-2 process (OCM), [kW]	671.22
Capital cost of steam turbine, [M£]	0.26

S. 1.4 Oxidative Coupling of Methane (OCM)

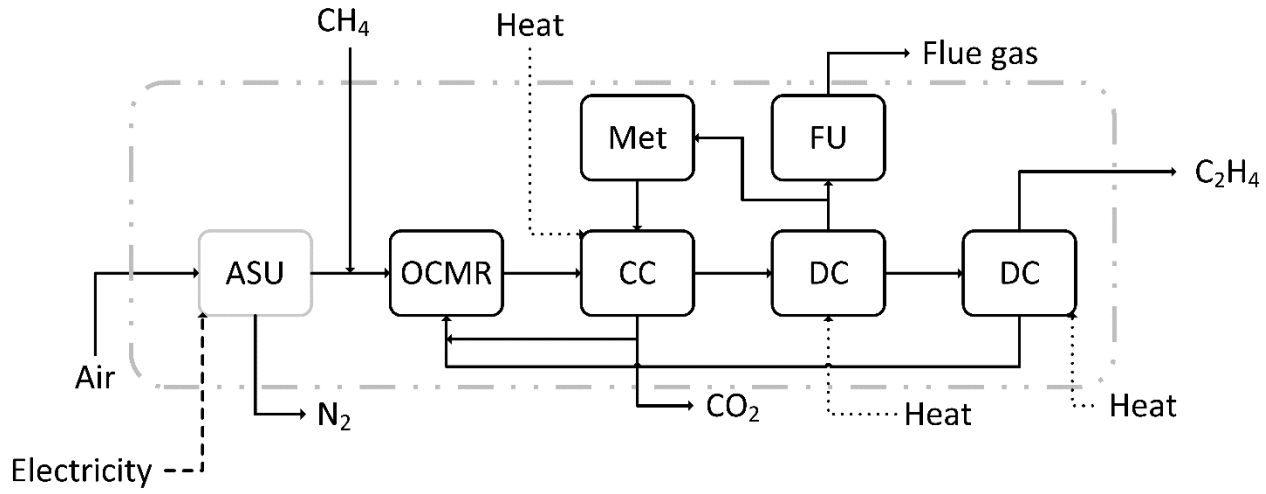

Figure S. 6: The block diagram of the oxidative coupling of methane process as described in Spallina et al. (8) *is shown. Oxygen from the cryogenic air separation unit (ASU) is mixed with the CH_4 feed stream before entering the OCM reactor (OCMR). Before feeding the product stream to the de-methanizer (DC), the CO_2 side-product is removed using a carbon capture unit (CC). The bottom product of the de-methanizer (DC) is fed to the de-ethanizer to obtain C_2H_4 with a purity of 99.5%. The top product is a CH_4 rich gas, that is partially purged and combusted in a boiler (FU), while the majority is sent to a methanator reactor (Met).*

The flowsheet as presented in Spallina et al. (8) remained unchanged, but an additional calculation was made to complete the mass balance around the OCM process and determine the emissions caused by the combustion of the purge stream (see Fig. S. 6). The composition of the flue gas was thereby determined based on a combustion calculation assuming 4% excess air. The mass balance around the boiler is given in Table S. 4.

Table S. 4: The mass balance around the boiler of the OCM process is summarised. The flue gas stream leaving the boiler results from the combustion of the CH_4 rich gas inlet stream in 4% excess air.

Chemical	**Molecular mass [g/mol]**	**CH_4 rich gas (inlet stream)**		**Flue gas (outlet stream)**	
		[kg]	[mol]	[kg]	[mol]
CH_4	16	10.20	0.64	-	-
CO	28	4.49	0.16	-	-
H_2	2	0.82	0.41	-	-
O_2	32	51.96	1.62	2.00	0.06
N_2	28	171.02	6.11	171.02	6.11
CO_2	44	-	-	35.11	0.80
H_2O	18	-	-	30.36	1.69
Total		238.49	8.94	238.49	8.66

S. 1.5 Syngas Fischer-Tropsch Synthesis (S-FT)

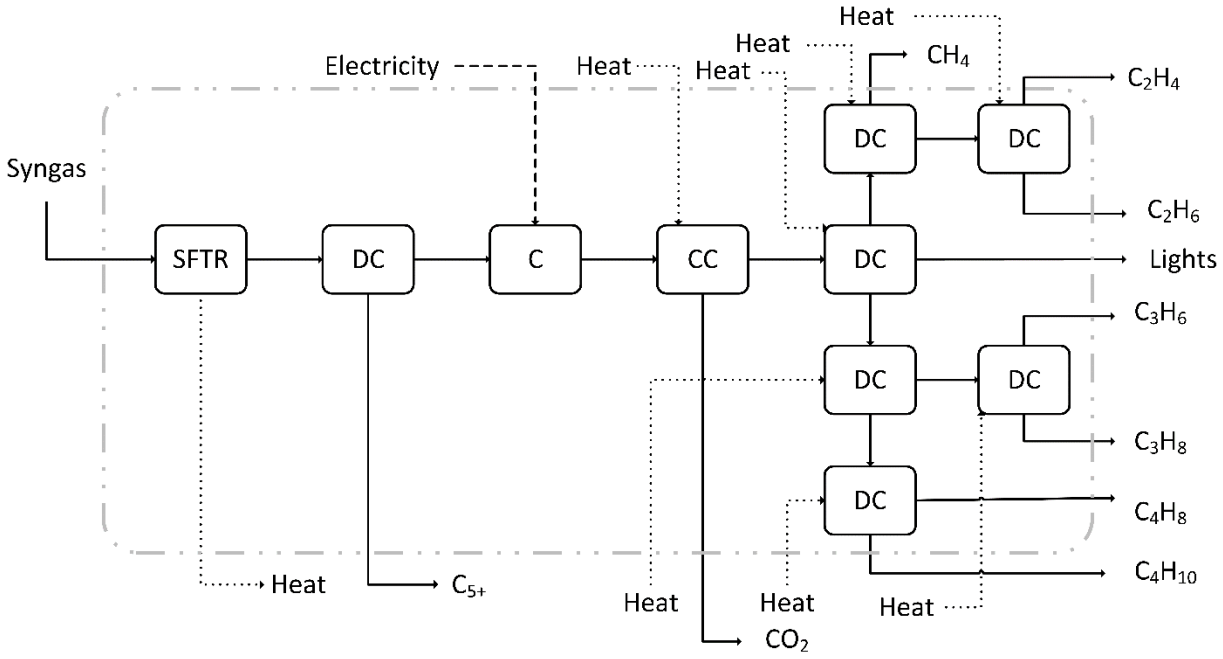

Figure S. 7: In the S-FT process presented in Liu et al. (9)*, the syngas feed stream is first converted to a mixture of short- and long-chain hydrocarbons in the Fischer-Tropsch reactor (SFTR). The heavier C_5 components are then removed in an extractive distillation (DC), before performing a CO_2 adsorption (CC) and separating the mixed product stream further in a cryogenic distillation train (DC units).*

The methane reformer used to produce syngas and the combined heat and power generator were excluded from the original flowsheet presented in Liu et al. (9). Therefore, the capital expenditures associated with these process units ($Cost_r$) were firstly back-calculated based on their base capacity (S_0), actual capacity (S_r), base unit capital cost ($Cost_0$) and scaling factor (s_f) using Eq. 4. Secondly, the CapEx summarised in Tab. S.5 were deducted from the direct costs of the overall process stated in Liu et al. (9)

$$Cost_r = 1.35 \cdot Cost_0 \left(\frac{S_r}{S_0}\right)^{s_f} \quad \text{(Eq. 4)}$$

Table S. 5: The process units removed from the original S-FT process of Liu et al. (9) *are summarised. The CapEx of the process units were determined using Eq. 4. The capacities of the CO_2 reformer and absorber are in [kg/s], while the capacities of the steam turbine and air compressor are given in [MW].*

Process unit	**Base unit cost, $Cost_0$ [M£]**	**Base capacity, S_0**	**Actual capacity, S_r**	**Scale factor, s_f [-]**	**CapEx, $Cost_r$ [M£]**
CO_2 reformer	19.62	12.2	17.64	0.67	39.79
Air compressor	3.85	8.54	5.04	0.67	4.28
Steam turbine	42.36	136	21.81	0.67	19.68
Amine-based CO_2 absorber	3.44	8.54	0.72	0.55	1.40

Upon removal of the process units summarised in Table S.4, excess heat from the Fischer-Tropsch reactor becomes available that can be used to generate electricity in a condensing steam turbine. The design of the steam turbine follows the procedure outlined in Section S. 1.2 and is summarised in Table S. 6.

Table S. 6: The excess process heat, generated electricity and capital cost of the steam turbine added to the S-FT process of Liu et al. (9) *are summarised. The electricity can be integrated with the stage-1 process producing the CO inlet stream of the S-FT process.*

Excess heat, [MWh]	19.89
Generated electricity, [MWh]	15.91
CapEx, [M£]	86.86

S. 1.6 Direct Fischer-Tropsch Synthesis (D-FT)

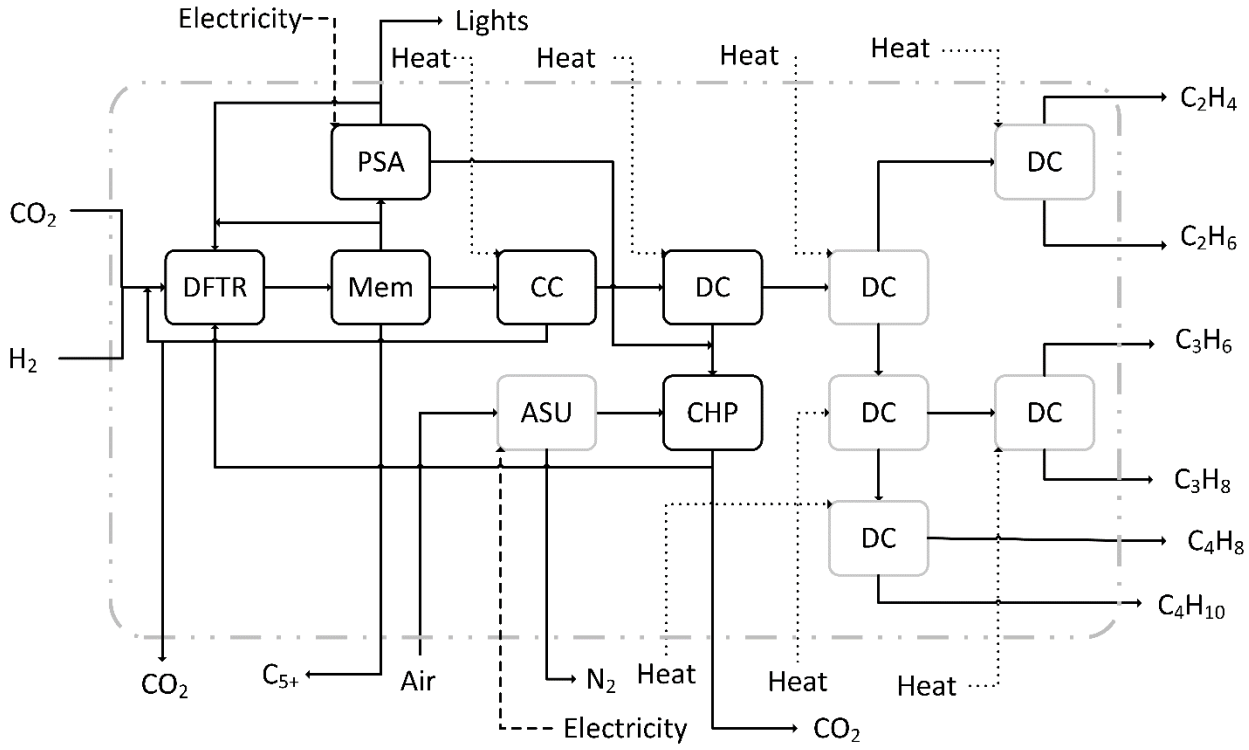

Figure S. 8: The direct Fischer-Tropsch process hydrogenates CO_2 to ethylene over a Fe-based catalyst. A major share of the unconverted CO_2 and H_2 are first recovered and using a membrane unit (Mem), before also using amine-based carbon capture unit (CC) to meet the specifications of the de-methanizer (DC). The pressure swing adsorption unit (PSA) recovers the H_2 in the permeate. A combined heat and power plant (CHP) generates utilities on-site from residue gas stream of the de-methanizer and PSA. The original D-FT flowsheet of Do and Kim (10) *is herein extended by a cryogenic distillation train (DC units) and an air separation unit (ASU).*

For our work, the process design for the D-FT synthesis from Do and Kim (10) was extended by including an air separation unit (ASU) to supply a pure O_2 stream to the combined heat and power plant (CHP) and a cryogenic distillation train comprising a de-ethanizer, C_2 distillation, $C_{3\text{-}4}$ splitter, C_3 distillation, and C_4 distillation column. The ASU is designed based on Gazzani et al. (11) with €1M for 0.35 t_{O2}/h and 8.1 kWh/t_{O2} as the reference values. The unit capacity and cost of the cryogenic distillation train were adopted from Liu et al. (9) and are summarised in Table S. 6. The actual costs are found using Eq. 4. The heat requirement (E_r) for a process is assumed to be linearly proportional to its actual capacity S_r and specific energy requirement (E_0/S_0) (Eq. 5).

$$E_r = \frac{E_0}{S_0} \cdot S_r \qquad \text{(Eq. 5)}$$

Table S. 7: For each distillation column of the cryogenic distillation train, the base capacity, base cost and scaling factor provided in Liu et al. (9) *is summarised. The actual capacity is determined based on the product stream in Do and Kim* (10)*. The capital costs are used to update the total capital investment cost of Do and Kim* (10)*.*

Process unit	**Base unit cost, $Cost_0$ [M£]**	**Base capacity, S_0**	**Actual capacity, S_r**	**Scale factor, s_f [-]**	**CapEx, $Cost_r$ [M£]**
De-methaniser	0.10	5.54	34.65	0.68	1.14
C_2 splitter	2.03	0.73	9.68	0.80	5.87
De-propaniser	0.68	1.14	24.61	0.79	0.74
C_3 splitter	1.45	0.65	12.74	0.64	3.13
C_4 splitter	1.79	0.40	11.87	0.82	3.59
Total					14.47

Table S. 8: The energy consumption of each distillation column of the cryogenic separation train as presented in Liu et al. (9) *is provided below. The energy demands were not integrated with the D-FT process in Do and Kim* (10)*.*

Process unit	**Base capacity, S_0**	**Actual capacity, S_r**	**Energy demand, E_0 [kW]**	**Actual energy demand, E_f [kW]**
De-methaniser	5.54	0.68	562.00	3,514.99
C_2 splitter	0.73	0.80	754.00	9,982.26
De-propaniser	1.14	0.79	537.00	11,594.91
C_3 splitter	0.65	0.64	2,346.00	45,854.00
C_4 splitter	0.40	0.82	1,141.00	33,653.59
Total				104,599.75

S. 2 Electrocatalytic Processes

S. 2.1 Process Modelling

S. 2.1.1 Low-Temperature Electrocatalytic Processes

Based on the experimental data, the electricity demand, electrode area and capital cost of the CO_2/CO electrolyser system need to be determined. The input parameters are the Faradaic efficiencies ($\eta_{F,i}$) of the individual products *i*, the conversion rate of CO_2 (or CO) (X_{CO_2}), the current density (j in A/m^2) and the half-cell reduction potential of CO_2 (or CO) (E_{red}^{SHE} in V). These parameters are tabulated in Table 1 of the publication. Additionally, the molar production rate of ethylene ($\dot{n}_{C_2H_4}$ in mol/s) at the chemical plant needs to be defined.

Using the Faradaic efficiency and molar production rate of ethylene, the electric current *I* in Ampere is determined using Eq. 6, where *F* is the Faraday constant of 96,485 As and z_i the number of electrons that are transferred per mole of product in the electroreduction as given by the reaction equations. The Faradaic efficiencies of the co-products of the electrocatalytic processes are summarised in Table S. 10.

$$\eta_{F,i} = \frac{z_i \cdot \dot{n}_i \cdot F}{I} \qquad \text{(Eq. 6)}$$

Table S. 10: The Faradaic efficiency of each co-product of the electrocatalytic processes are listed below. Abbreviations: eCO: CO_2 electroreduction to carbon monoxide; eCH$_4$: CO_2 electroreduction to methane; S-eC$_2$H$_4$: CO electroreduction to ethylene; D-eC$_2$H$_4$: CO2 electroreduction to ethylene.

Process	**Ref.**	**Faradaic efficiency of individual product *i*, $\eta_{F,i}$ [-]**							
		CO	H_2	CH_4	HCOOH	C_2H_4	C_2H_5OH	C_3H_7OH	CH_3COOH
eCO	(12)	0.998	0.002	-	-	-	-	-	-
eCH$_4$	(13)	0.02	0.14	0.73	-	0.05	-	-	-
S-eC$_2$H$_4$	(14)	-	0.07	-	-	0.69	0.15	0.02	0.11
D-eC$_2$H$_4$	(15)	0.03	0.31	-	-	0.66	-	-	-

According to the conversion rate achieved in the experiments, the input stream of CO_2/CO must be greater than the stoichiometrically required molar flow rate ($\dot{n}_{CO_2}^{st}$).

$$X_{CO_2} = \frac{\dot{n}_{CO_2}^{st}}{\dot{n}_{CO_2}} \qquad \text{(Eq. 7)}$$

The necessary power applied to the CO2/CO electrolyser results from the electric current *I* and the cell voltage E_{cell} (Eq. 8).

$$P = I \cdot E_{cell} \quad \text{(Eq. 8)}$$

For the half-cell voltage, the overpotential given in the relevant references (see Table S.11) is converted from their reference electrode to the SHE (Eq. 9-10).

$$E_{red}^{SHE} = E_{red}^{RHE} + 0.059 \cdot pH \quad \text{(Eq. 9)}$$

$$E_{red}^{SHE} = E_{red}^{SCE} + 0.2415 \quad \text{(Eq. 10)}$$

The cell voltage is now calculated by adding the half-cell potentials of the CO_2/CO reduction and the oxygen evolution reaction (OER) (Eq. 11).

$$E_{cell} = E_{red,CO2/CO} - E_{red,OER} \quad \text{(Eq. 11)}$$

The actual half-cell potentials deviate from the standard cell potentials due to overpotentials needed to overcome the ohmic resistance at high current densities and kinetically activate the electrodes. For the cathode, we assume the overpotential to be included in the experimental measurements of the half-cell potentials for the CO_2/CO electroreduction. However, for the anode, an overpotential (ΔE_{OP}) of 0.8 V as determined in (16) is added on top of the standard reduction potential for the OER under alkaline conditions ($E_{red,OER}^{0}$) of 0.4 V. The half-cell potentials for the CO_2/CO electroreduction under alkaline conditions to the different co-products of the electrocatalytic processes are reported in Table S.11.

Table S.11: The half-cell potential for each co-product of the CO/CO_2 electroreduction under alkaline conditions is given below.

Ref.	Half-cell Electrochemical Reaction	Potential E_{red} [V]	Reference Electrode
(12)	$CO_2 + 2\ H_2O + 2\ e^- \rightarrow CO + 2\ OH^-$	-0.11	RHE
(17)	$CO_2 + 6\ H_2O + 8\ e^- \rightarrow CH_4 + 8\ OH^-$	-0.13	SCE
(17)	$CO_2 + H_2O + 2\ e^- \rightarrow HCOOH + 2\ OH^-$	-0.61	SCE
(15)	$2\ CO_2 + 8\ H_2O + 12\ e^- \rightarrow C_2H_4 + 12\ OH^-$	0.08	RHE
(14)	$2\ CO + 4\ H_2O + 8\ e^- \rightarrow C_2H_4 + 8\ OH^-$	0.59	RHE
(14)	$2\ CO + 6\ H_2O + 8\ e^- \rightarrow C_2H_5OH + 6\ OH^-$	0.09	RHE
(14)	$2\ CO + 8\ H_2O + 12\ e^- \rightarrow C_3H_7OH + 12\ OH^-$	0.10	RHE
(14)	$2\ CO + 2\ H_2O + 2\ e^- \rightarrow CH_3COOH + 2\ OH^-$	0.11	RHE
(18)	$8\ OH^- \rightarrow 2\ O_2 + 4\ H_2O + 8\ e^-$	0.4	SHE

As electrochemical reactions occur on the interface of the electrodes, the reaction rate is proportional to the electrode area (A_{cell}). Based on the current density *j* and the calculated total current *I*, the electrode area can be determined.

$$j = \frac{I}{A_{cell}} \quad \text{(Eq. 12)}$$

Higher current densities decrease the overall electrolyser size. In general, *j* is a function of the mass transfer from and to the electrode surface, the adsorption of CO_2/CO to the catalyst, the kinetics of the electron transfer, and the reaction mechanism.

While experiments on CO_2/CO electrolysis are commonly performed in H-type and flow cells, a zero-gap arrangement in which the cathodic and anodic porous transport layers are in direct contact with the catalyst coated ion-exchange membrane is expected to be used for large-scale CO_2/CO electrolysers, because it reduces the ohmic resistance and of its smaller ohmic resistance and tolerates pressurised inlet streams (19,20). The humidified CO_2 (or CO) stream is fed directly to the cathodic gas diffusion electrode, while deionised water or an aqueous hydroxide solution is at the anode. For the electroreduction of CO_2 (CO_2RR) or CO (CORR), anion exchange membranes (AEM) are preferred because the acidic conditions of a proton exchange membrane (PEM) favour the hydrogen evolution reaction (HER) at the cathode (20). The milder reaction conditions of AEM electrolysers allow for the use of cheaper metals such as copper or silver at the cathode and Fe_2O_3/NiO at the anode instead of corrosion-resistant but expensive platinum-group metals (21,22). However, 0.01-0.1 M KOH solutions are required to achieve pH > 9 in the anolyte to stabilise the transition-metal catalyst (21,23). Currently, AEM such as Sustainion (24) and PiperION (25) are being developed for CO_2RR but at high costs of 3001.3 £/m^2 (123) caused by their small scale of production. Note, that low-temperature AEM-based CO_2RR suffer from parasitic losses due to the (bi-)carbonate formation (26), but these losses had to be neglected as they are not quantified in the experiments underlying our CO_2 electrolyser models. However, this assumption leads to a general overestimation of the energy efficiency (27).

Having qualitatively assessed the future design of large-scale low-temperature CO_2/CO electrolysers, their capital costs are derived based on analogies to existing electrolyser technologies: The cell design and the balance of plant (BOP) layout of AEM electrolysers are found to be similar to PEM electrolysers (28). While the same cost structure for the capital cost of the electrolyser stack is assumed, the difference in the catalyst coated membrane (CCM) is accounted for (see Table S. 12). To estimate the cost of the CO2 electrolyser stack, the mass loading of Ag catalyst from Moreno-Gonzalez et al. (29) is assimilated to a Cu catalyst at the cathode side. The future price of the anion-exchange membrane itself is set to match the large-scale production price of the Nafion™ membranes (352.4 £/m^2) commonly used in PEM electrolysers (28,30). The capital cost of the CCM ($Cost_{CCM}$) is projected to be responsible for f_{CCM}= 45% of the stack cost in future PEM electrolysers (30). Based on A_{cell} determined in Eq. 12, the electrolyser stack of a low-temperature CO_2/CO electrolyser ($Cost_{stack,LT}$) can hence be calculated by Eq. 13.

$$Cost_{stack,LT} = \frac{1}{f_{CCM}} \cdot Cost_{CCM} \cdot A_{cell} \qquad \text{(Eq. 13)}$$

Table S. 12: Based on the method of Moreno-Gonzalez et al. (29)*, the capital cost of the catalyst coated membrane ($Cost_{CCM}$) are determined based on the catalyst loading and cost* (29,31)*. The cost of the AEM in CO_2/CO electrolysers is set equal to the price of Nafion membranes* (28,30)*.*

Building block	Loading [g/m2]	Cost [£2019/kg]	Cost/Area [£2019/m^2]
Cathode: Cu-catalyst	0.1	4.72	0.047
Anode: Fe_2O_3/NiO	0.2	811.72	16.23
Membrane: Nafion			352.42
TOTAL $Cost_{CCM}$			368.70

For the present value of the total CO_2/CO electrolyser cost ($Cost_{system,LT}$) (see Eq. 14), the additional cost of the BOP ($Cost_{BOP}$) and the discounted cost of the stack replacements need to be accounted for. The BOP comprises the power supply, deionised water circulation system, hydrogen processing and cooling equipment, with the specific BOP cost ($SC_{BOP,LT}$) being set to 105.7 £/kW (30). By 2035, we assume the lifetime (LT) of the electrolyser stack to have extended to 5 years, leading to a total of 4 stack replacements ($s = 0,..,S-1$ with $S = 4$) over the 20-year lifetime of the chemical plant.

$$Cost_{system,LT} = \frac{1}{f_{UF}}\left(SC_{BOP,LT} \cdot P + Cost_{stack,LT} \cdot \sum_{s=0}^{S-1} \frac{1}{(1+r)^{LT \cdot s}}\right) \quad \text{(Eq. 14)}$$

As the BOP already comprises the majority of piping, instrumentation, and electrical installation, only equipment erection ($f_{er} = 0.3$), civil engineering ($f_c = 0.3$), and structures and buildings ($f_{sb} = 0.2$) (32) are added as indirect cost to the equipment cost to derive the fixed capital investment (FCI) of the electrolyser ($Cost_{FCI,EL}$):

$$Cost_{FCI,EL} = (1 + f_{er} + f_c + f_{sb}) \cdot Cost_{system,LT} \quad \text{(Eq. 15)}$$

To separate the gaseous products streams of the CO_2/CO electrolyser, a separation train is designed. To recover and recycle any unconverted CO_2, a mixed-amine (MA) CO_2 absorption with a capture rate of 97% is applied first (33). The sequence of the subsequent separation units is dependent on the composition of the product stream. Ethylene can be separated from a mixture of H_2/CO/C_2H_4 by using a five-bed vacuum pressure swing adsorption (VPSA) with zeolite CaX (34). However, to separate H_2, CO and C_2H_4 with good purity and recovery, two separation stages are needed: H_2 is removed first using a five-bed VPSA with activated carbon (35) and only afterwards a five-bed vacuum pressure swing adsorption (VPSA) with zeolite CaX can be used to separate CO and C_2H_4. The VPSA model by Ramdin et al. (2021) is thereby adjusted to take the higher cost of CaX adsorbent into account.

A minimum concentration of 20 wt% in the electrolyte is required, before the liquid side-products such as acetic acid and alcohols (methanol, ethanol, propanol) can be separated (35). Acetic acid are separated by a liquid-liquid extractor using ethyl acetate, followed by an azeotropic distillation obtaining acetic acid as a bottom product. The separation of formic acid is assumed to proceed

analogously. For any of the alcohols, a two-stage distillation train can be used. The explicit separation train for each of the electrocatalytic processes is shown in the process diagrams of Section 2.2. The reference capacity (S_0), capital cost (C_0), and utility demands of the separation processes are summarised in Table S. 13. The utility requirement is assumed to scale linearly with the capacity of the separation unit, while the capital cost follows the economies of scale with a scaling factor (n) of 0.6 (see Eq. 16). However, given limits on diameter and pressure drop over an adsorption column, the feed is limited to a maximum volumetric flow rate of 21.6 m^3/s (36). In the fixed capital costs of the separation process ($Cost_{FCI,SP}$), the indirect cost for piping, engineering and construction are included (f_{IC} = 2.2) (32).

$$Cost_{FCI,SP} = (1 + f_{IC})C_0 \left(\frac{S}{S_0}\right)^n \quad \text{(Eq. 16)}$$

The fixed capital cost of the full electrocatalytic process ($Cost_{FCI,tot}$) is then determined by Eq. 17.

$$Cost_{FCI,tot} = Cost_{FCI,EL} + Cost_{FCI,SP} \quad \text{(Eq. 17)}$$

Having determined the fixed capital investments for the CO_2/CO electrolyser and its associated separation train ($Cost_{FCI,tot}$), the total invested capital (TIC) (37) can be determined by including additional costs incurred for the working capital needed to finance everyday operation ($Cost_{WC}$), plant start-up ($Cost_{start}$) and contingencies ($Cost_{cont}$):

$$Cost_{TIC} = Cost_{FCI,tot} + Cost_{WC} + Cost_{start} + Cost_{cont} \quad \text{(Eq. 18)}$$

$Cost_{WC}$, $Cost_{start}$, and $Cost_{cont}$ are 15% (2), 10% (38) and 10% (32) of $Cost_{FCI,tot}$, respectively. The outside battery limit (OSBL) costs are neglected as the new production plant is assumed to replace a fossil-based process plant and therefore have the relevant infrastructure already in place. As in the case of the thermocatalytic process models, heat is supplied by hydrogen boilers, while the electricity demand is met through renewable electricity imports as the separation train cannot be integrated with the low-temperature electrolysers.

Table S. 13: The key characteristics of the separation processes are summarised.

Separation process	Ref.	Capacity S_0 [Mt/y]	CapEx C_0 [M£2019]	Electricity demand [MW]	Heat demand [MW]
MA CO2 Absorption	(33)	529.57	148.60	-	53.26
EtVSA	(39)	5.08	4951.95	136.64	-
H_2VPSA	(35)	0.02	2.34	0.33	-
Liquid-liquid Extractor	(35)	0.15	10	0.6	-

S. 2.1.2 High-Temperature Electrocatalytic Processes

The model of the HT CO electrolyser is based on the total energy consumption of 6-8 kWh per Nm^3 CO as stated by Haldor Topsoe (40). The upper limit was assumed to be applicable for a CO product stream with high purity (>99.5 vol%). According to Haldor Topsoe (40), 1 Nm^3 of CO_2 is consumed per 1 Nm^3 CO, which is accomplished using an internal recycle stream after separation (41) and translates into an overall conversion of 100% with a Faradaic efficiency of 100%. Based on the CO feed to the stage-2 process (see S. 6.4 and S. 6.5), the electricity consumption and CO_2 feed rate can be calculated. The oxygen production rate follows from the stochiometric reaction equation and the CO production rate.

Similar to the approach chosen for costing the low-temperature CO_2 electrolysers, the high-temperature CO electrolyser is assumed to indirectly benefit from the scale-up of their high-temperature counterparts for H_2 production. The capital cost of the SOEC is determined based on the specific system cost ($SC_{HT,ref}$) assumed for 2035 (600 £/kW (42)) and the power consumption of the HT eCO process. The stack cost is thereby estimated to contribute 21-26% of the system cost in the future (43,44). For simplicity, we herein assume 25% ($f_{HT,stack}$).

$$Cost_{stack,HT} = f_{HT,stack} \cdot SC_{HT,ref} \cdot P \qquad \text{(Eq. 19)}$$

Aligned with the assumptions made for LT CO_2/CO electrolysers, the stack lifetime (LT) is assumed to reach 5 years by 2035 (44,45). Hence, 4 stack replacements ($S = 4$) will take place over the 20-year lifetime of the chemical plant as stated in Eq. 20 ($s = 0, .., S-1$):

$$Cost_{system,HT} = (1 - f_{HT}) \cdot SC_{HT,ref} \cdot P + Cost_{stack,HT} \cdot \sum_{s=0}^{S-1} \frac{1}{(1+r)^{LT \cdot s}} \qquad \text{(Eq. 20)}$$

The BOP of the SOEC already comprises the majority of piping, instrumentation, and electrical installation. For the fixed capital investment (FCI) of the HT CO electrolyser ($Cost_{FCI,EL}$) only equipment erection ($f_{er} = 0.3$), civil engineering ($f_c = 0.3$), and structures and buildings ($f_{sb} = 0.2$) (32) are therefore added as indirect cost to the system cost:

$$Cost_{FCI,EL} = (1 + f_{er} + f_c + f_{sb}) \cdot Cost_{system,HT} \qquad \text{(Eq. 21)}$$

S. 2.2 Electrocatalytic Processes including Product Separation

For each of the electrocatalytic processes, a process block diagram of the overall process is provided, and a stream table is used to summarise the mass balances around the individual process units. The process comprises the CO_2/CO electrolyser and the separation processes required to purify the product and recycle the unconverted CO_2/CO.

S. 2.2.1 CO_2 Electroreduction to Methane (eCH_4)

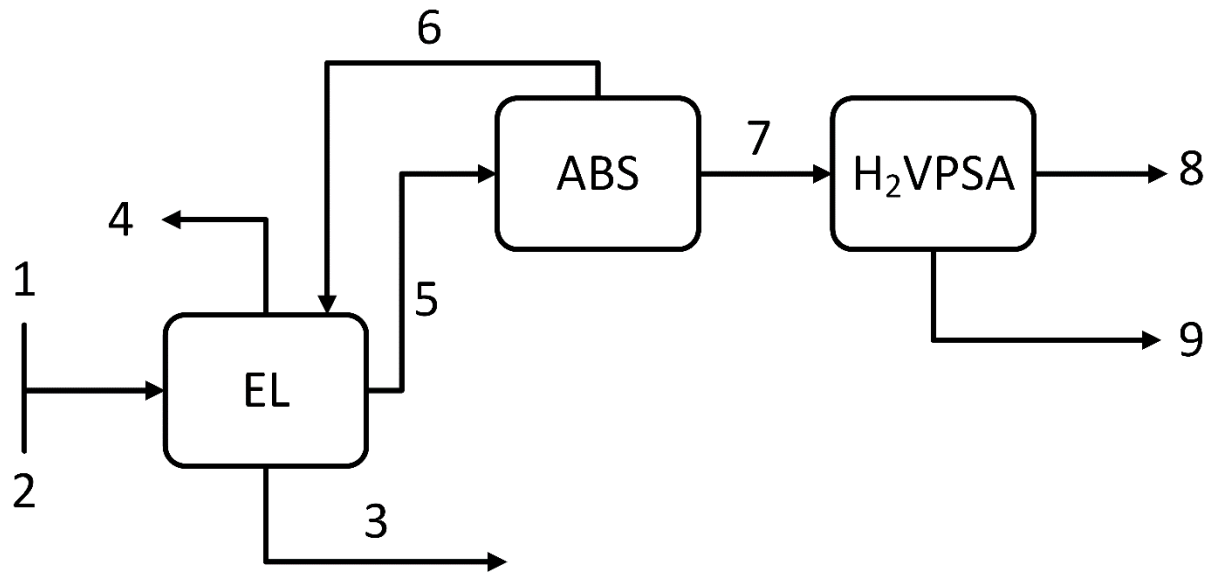

Figure S.9: In the CO_2 electrolyser of the eCH_4 process, CO_2 (1) and water (2) are converted to oxygen (4) and a mixed product stream (5) of methane, formic acid and H_2 with 82 wt% of unconverted CO_2. The latter is separated in an absorption column (ABS) before being recycled. The methane product is purified to 95 wt% using a vacuum pressure swing adsorption (H_2VPSA).

Table S. 14: The stream table summarises the mass balances around the CO_2 electrolyser and separation units of the eCH_4 process. Stream 8 represents the product stream that is integrated with the stage-2 process to produce ethylene.

Chemical	**Mass of product j in stream i**								
	1	**2**	**3**	**4**	**5**	**6**	**7**	**8**	**9**
CO_2	4.14				5.41	5.24	0.17		0.17
H_2O		6.16	2.83						
O_2				5.48					
CH_4					1.00		1.00	1.00	
C_2H_4					0.18		0.18	0.18	
H_2					0.10		0.10		0.03

S. 2.2.2 Direct CO_2 Electroreduction to Ethylene (D-eC_2H_4)

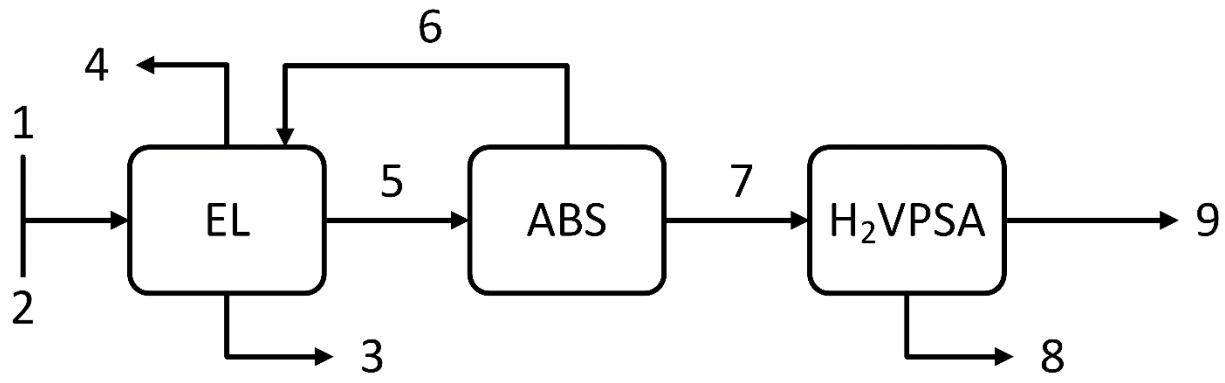

Figure S. 10: The product stream (5) of the direct electroreduction of CO2 (1) to ethylene is purified to 79 wt% C_2H_4 (9) by separating and recycling the unconverted CO_2 (6) first and then removing the hydrogen by-product (8) using vacuum pressure swing adsorption (H_2VPSA).

Table S. 15: The mass balances around the CO_2 electrolyser and separation units are summarised in form of a stream table. Wastewater (3), oxygen (4), hydrogen (8) and the ethylene product stream (9) are leaving the system boundary, while CO_2 (1) and fresh water (2) enter it.

Chemical	**Mass of product j in stream i**								
	1	**2**	**3**	**4**	**5**	**6**	**7**	**8**	**9**
CO_2	3.49				4.27	4.14	0.13		0.13
H_2O		4.85	2.66						
O_2				4.31					
C_2H_4					1.00		1.00		1.00
CO					0.14				0.14
H_2					0.10		0.10	0.10	

S. 2.2.3 CO Electroreduction to Ethylene (S-eC_2H_4)

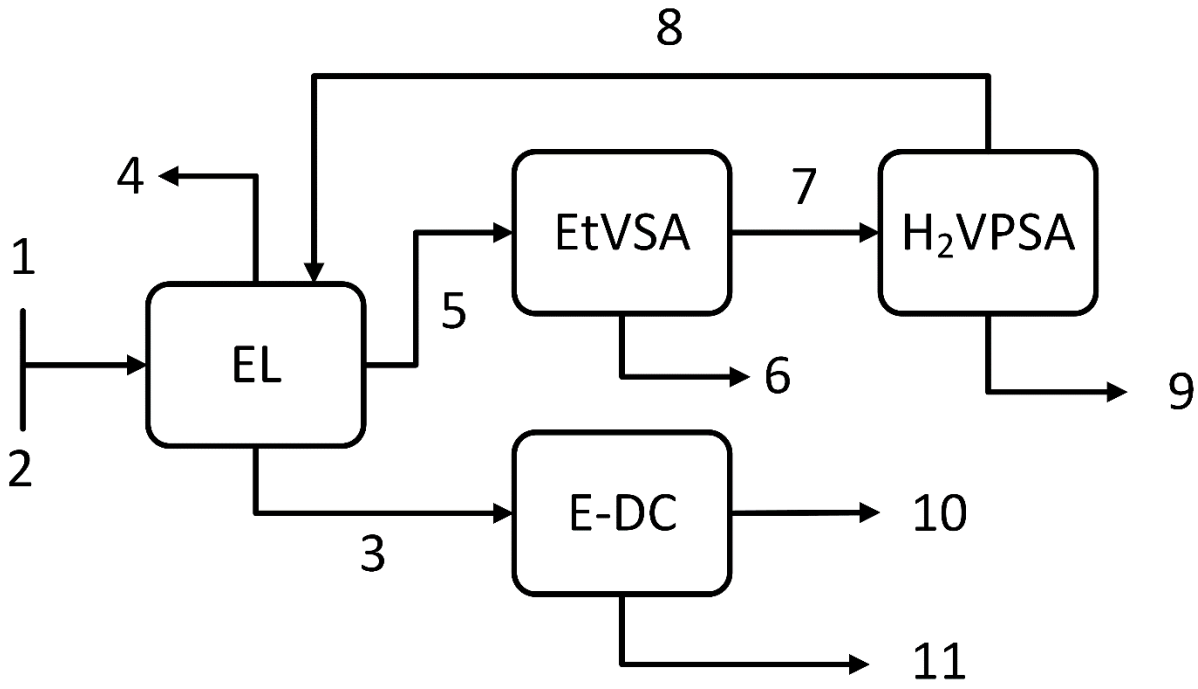

Figure S. 11: The S-eC_2H_4 process uses a CO electrolyser (EL) to convert CO (1) and water (2) to a mixture of ethylene, minor H_2 impurities and 79 wt% of unconverted CO (5). Ethylene and syngas are separated in a vacuum pressure swing adsorption (EtVPSA) with CaX type zeolite, leading to product stream (6) with 89 wt% ethylene. Using a second VPSA (H_2VPSA), the unconverted CO is separated and recycled to the electrolyser (8). Alcohols formed as liquid side products (3) are removed from the wastewater stream in an extractive distillation (E-DC).

Table S. 16: The mass balance for each process unit of the S-eC_2H_4 process can be calculated based on the stream table below. Stream (6) represents the ethylene product stream. Acetic acid, ethanol and ethanol are the liquid co-products in Stream (3).

Chemical	**Mass of product j in stream i**										
	1	**2**	**3**	**4**	**5**	**6**	**7**	**8**	**9**	**10**	**11**
CO	3.25				3.98	0.12	3.86	3.86			
H_2O		3.88	1.45								3.88
O_2				3.45							
C_2H_4					1.00	1.00					
CH_3COOH			0.68							0.68	
CH_3CH_2OH			0.36							0.36	
$CH_3CH_2CH_2OH$			0.04							0.04	
H_2					0.03		0.03		0.03		

S. 2.2.4 CO_2 Electroreduction to Carbon Monoxide (eCO)

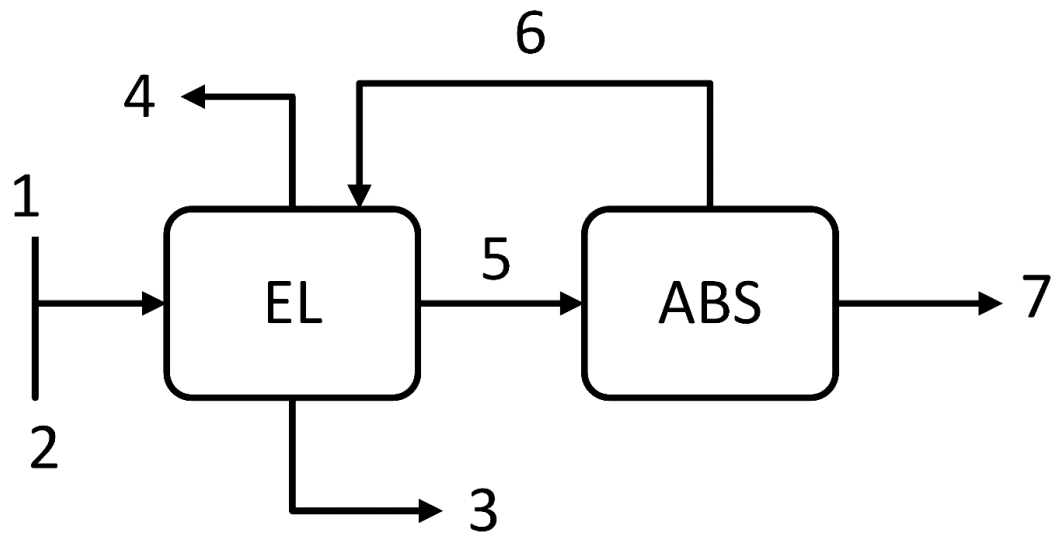

Figure S. 12: The CO_2 feedstock (1) is reduced to CO leaving the CO_2 electrolyser (EL) as a 1:5 mixture of CO/CO_2 (5), that is separated in an absorption column (ABS). The unconverted CO_2 is recycled (6).

Table S. 17: The stream table provides an overview on the mass balances for each process unit of the eCO process. The CO content in the product stream (7) is 68 wt%.

Chemical	**Mass of product j in stream i**						
	1	**2**	**3**	**4**	**5**	**6**	**7**
CO_2	2.04				4.71	4.24	0.47
H_2O		0.64	0.64				
O_2				0.57			
CO					1.00		1.00
H_2					0.00		0.00

S. 2.2.5 Exclusion of Liquid Product from eCH_4 and S-eC_2H_4 processes

S-eC_2H_4 process liquid co-products alongside their target products methane and ethylene, respectively. For the rough calculations described in the following, the density of the liquid products and the electrolyte are set equal for simplicity.

The reference electrolyser for the S-eC_2H_4 process by Ji et al. (14) uses a flow-cell set-up in which the electrolyte flows. Like Ramdin et al. (35), we assume that a concentration of 20 wt% formic acid in the aqueous electrolyte is required for the separation in an extractive distillation column. Therefore, the electrolyte needs to be recycled before the overall liquid product concentration reaches 20 wt%. Using the Faradaic efficiencies and current density reported in Ji et al. (14), the single-pass concentration for each liquid product is determines in Table S. 19. Also here, the liquid products are hence neglected.

Table S. 29: For the S-eC_2H_4 process (14)*, the concentration of the liquid co-products for a single-pass of the electrolyte is determined, justifying their exclusion from the valuable co-products.*

	Liquid product		
	Acetic acid	**Ethanol**	**Propanol**
Stack area, cm^3	13		
Current density, $mA\ cm^{-3}$	150		
Faradaic efficiency	0.11	0.15	0.02
$\dot{m}_{product}, g\ min^{-1}$	$1.05 \cdot 10^{-3}$	$7.89 \cdot 10^{-4}$	$8.03 \cdot 10^{-5}$
$\dot{V}_{product}, cm^3\ min^{-1}$	0.001	0.001	0.0001
$\dot{V}_{electrolyte}, cm^3\ min^{-1}$	0.5		
$Concentration, vol\%$	0.002	0.002	0.0002

S. 2.2.6 Fixed Capital Investment of the Low-Temperature Electrocatalytic Processes

Table S. 20: The power, area, stack cost, system cost and fixed investment cost of each low-temperature electrocatalytic process as part of each production route to ethylene.

Processes	**P [MW]**	**A [m^2]**	$Cost_{stack}$ **[M£$_{2019}$]**	$Cost_{system}$ **[M£$_{2019}$]**	$Cost_{FCI,EL}$ **[M£$_{2019}$]**
eCO (eCO + S- eC_2H_4)	1619.40	163,666.55	134.10	595.90	1072.61
eCO (eCO + S-FT)	17840.94	1,803,116.38	1477.35	6565.00	11817.00
S-eC_2H_4 (eCO + S- eC_2H_4)	2844.91	675,670.23	553.60	2009.01	3616.22
S-eC2H4 (HT-eCO + S- eC_2H_4)	2844.91	675,670.23	553.60	2009.01	3616.22
D- eC_2H_4	4175.02	1,444,873.33	1183.83	4071.98	7329.56
eCH_4 (eCH_4 + OCM)	13932.61	794,107.38	650.64	3604.79	6488.63

S. 3 Olefin Production in the UK

Table S. 21: For each olefin production plant in the UK, the location, capacity, and production technology are provided. The plant in Wilton serves as a case study for our analysis (see Section 2.4 of the main manuscript).

Company	Location	Technology	Capacity, $t\ yr^{-1}$	Ref
Sabic	Wilton	Ethane cracking	800,000	(46,47)
ExxonMobil	Fife		800,000	(48)
Ineos	Grangemouth	Mixed alkane cracking	700,000	(49)

S. 4 Economic Allocation Factor versus Cash Flow Analysis

The cash flow method often used in economic analyses and the economic allocation factor used in our work are in the following shown to be identical:

The levelised cost of ethylene with a constant annual cash flow is

$$LCOEt = \frac{OpEx + CapEx \cdot CRF - Revenue}{m_e}. \quad \text{(Eq. 22)}$$

Revenue can be expressed as a function of LCOEt as

$$Revenue = \sum Cost_j \cdot m_j = LCOEt \cdot \sum \frac{Cost_j}{LCOEt} \cdot m_j = LCOEt \cdot \sum r_j \cdot m_j. \quad \text{(Eq. 23)}$$

Thus,

$$LCOEt + \frac{LCOEt \cdot \sum r_j \cdot m_j}{m_e} = \frac{OpEx + CapEx \cdot CRF}{m_e} \quad \text{(Eq. 24)}$$

$$LCOEt = \frac{OpEx + CapEx \cdot CRF}{m_e} \cdot \frac{1}{1 + \frac{\sum r_j \cdot m_j}{m_e}} \quad \text{(Eq. 25)}$$

$$= \frac{OpEx + CapEx \cdot CRF}{m_e} \cdot \frac{m_e}{m_e + \sum r_j \cdot m_j}, \quad \text{(Eq. 26)}$$

i.e. a scaling factor of

$$\frac{m_e}{m_e + \sum r_j \cdot m_j} = AF_{econ}. \quad \text{(Eq. 27)}$$

S. 5 Techno-Economic Assessment

The capital expenditures ($CapEx$), as described in Sections 2.1.1 and 2.1.2 of the publication, are annualised using a uniform Capital Recovery Factor (CRF, Eq. 25) with interest rate r over the plant lifetime LT (50).

$$CRF = \frac{r(1+r)^{LT}}{(1+r)^{LT}-1} \quad \text{(Eq. 28)}$$

The operational expenditures ($OpEx$, Eq. 26) comprise the variable utility costs and the fixed operating expenses for salaries (3%), maintenance (3%) and overheads (1%) ($f_{O\&M}$). The former are proportional to the annual production (m_k) and unit price ($Cost_k$) of each input and process emission $k \in \{CO_2, H_2, \text{el}, \text{ww}, \text{tax}\}$. The latter is set to 7% of the capital costs and assumed constant throughout the plant's lifetime (32).

$$OpEx = f_{O\&M} CapEx + \sum_k m_k Cost_k \quad \text{(Eq. 29)}$$

The revenue of each co-product $j \in \{CH_4, C_2H_6, C_3H_8, C_3H_6, C_{4+}, O_2\}$ is determined by its market price ($Price_j$) and annual production (m_j). Similarly, the revenue from selling ethylene is given by its market price ($Price_{C2H4}$) and annual production (m_{C2H4}). The general expression of AF_j is given in Eq. 27.

$$AF_j = \frac{m_j Price_j}{\sum_j m_j Price_j} \quad \text{(Eq. 30)}$$

In this work, the market price of the green co-products is assumed to increase alongside the price of green ethylene but their ratio ($Ratio_j$, Eq. 2 in the main text) is assumed to remain constant. Therefore, Eq. 27 is reformulated as a function of the price ratio between the co-products and ethylene in Eq. 3 of Section 2.2 in the publication.

S. 6 Detailed Energy and Mass Balances

The following tables provide the detailed mass and energy balances underlying the process inventories presented in Fig. 2 of the main manuscript. Inlet streams to the process carry a positive sign while outlet streams have negative signs. The production target is 1 tonne of ethylene and where applicable, the stage-1 process supplying the intermediate to the stage-2 process is scaled accordingly. As the stage-1 and stage-2 process are integrated, the process inventories only represent the net in- and outflow of the coupled processes. The capital expenditures are calculated for the ethylene production plant in Wilton (UK) with a capacity of 800 kt per year (see Section S. 3).

S. 6.1 MS + MTO

Table S.22: Detailed mass and energy balances of the MS & MTO process.

Stream	Unit	Process	
		MS	**MTO**
CO_2	$t\ t_e^{-1}$	8.87	-0.08
Air		4.92	
H_2O			1.52
MeOH		**-6.07**	**6.07**
Ethylene			**-1.00**
Ethane			-0.02
Propylene			-1.01
Propane			-0.01
C_{4+}			-0.52
CH_4			-0.06
CO			-0.01
CO_2		-0.55	
Wastewater		-3.49	-4.85
Electricity	$MWh\ t_e^{-1}$	1.03	0.52
H_2 Heat		0.23	0.84
H_2 Feed		47.70	
CapEx	M£	753.00	418.67

S. 6.2 CTM + OCM

Table S.23: Detailed mass and energy balances of CTM & OCM. The composition of the total intermediate stream is provided.

Stream	Unit	Process	
		CTM	**OCM**
CO_2	$t\ t_e^{-1}$	5.71	-1.12
Air			23.70
H_2O			6.10
Total stream of intermediate		**-2.37**	**2.37**
CH_4		-1.94	2.37
CO_2		-0.31	
H_2O		-0.02	
H_2		-0.07	
O_2			
CO_2			-1.1
Ethylene			**-1.00**
Wastewater		-4.41	-9.79
Electricity	$MWh\ t_e^{-1}$	-4.83	4.24
H_2 Heat			
H_2 Feed		41.84	
CapEx	M£	361.76	851.11

S. 6.3 eCH_4 + OCM

Table S.24: Detailed mass and energy balances of eCH4 & OCM. The composition of the total intermediate stream is provided.

Stream	Unit	Process	
		eCH_4	**OCM**
CO_2	$t\ t_e^{-1}$	7.33	-1.12
Air			23.70
H_2O		10.91	6.10
Total stream of intermediate		**-2.37**	**2.37**
CH_4		-1.96	2.37
CO_2		-0.40	
H_2O			
H_2			
O_2		-9.70	
Ethylene			**-1.00**
CO_2		-1.1	
Wastewater		-4.60	-9.79
Electricity	$MWh\ t_e^{-1}$	152.87	4.24
H_2 Heat		4.75	
H_2 Feed			
CapEx	M£	6952.22	851.11

S. 6.4 eCO + S-FT

Table S.25: Detailed mass and energy balances of the eCO and S-FT process.

Stream	Unit	Process	
		eCO	**S-FT**
CO_2	$t\ t_e^{-1}$	49.16	-17.87
H_2O		17.52	
Syngas stream		**-36.04**	**36.04**
H_2		-2.41	2.41
CO		-33.63	33.63
O_2		-15.58	
Ethylene			**-1.00**
Ethane			-0.85
Propylene			-1.58
Propane			-0.28
butene			-0.75
butane			-0.27
C_{4+}			-2.27
CH_4			-9.28
CO_2			-8.79
Wastewater		-15.58	-5.76
Electricity	$MWh\ t_e^{-1}$	182.29	-15.91
H_2 Heat		70.74	
H_2 Feed		94.80	
CapEx	M£	11943.42	1612.80

S. 6.5 eCO + S-eC_2H_4

Table S. 26: Detailed mass and energy balances of the eCO and S-eC_2H_4 processes.

Stream	Unit	Process	
		eCO	**S-eC_2H_4**
CO_2	$t\ t_e^{-1}$	4.78	
H_2O			3.32
CO		**-2.77**	**2.77**
O_2		-1.51	-3.45
Ethylene			**-1.00**
CO_2			-1.05
Wastewater		-1.70	-2.53
Electricity	$MWh\ t_e^{-1}$	18.00	31.15
H_2 Heat		3.80	
CapEx	M£	1125.01	3759.55

S. 6.6 HTeCO + S-FT

Table S. 27: Detailed mass and energy balances of the HTeCO and S-FT processes.

Stream	Unit	Process	
		HTeCO	**S-FT**
CO_2	$t\ t_e^{-1}$	52.81	-17.87
H_2O			
Syngas stream		**-36.04**	**36.04**
H_2		-2.41	2.41
CO		-33.63	33.63
O_2		-19.18	
Ethylene			**-1.00**
Ethane			-0.85
Propylene			-1.58
Propane			-0.28
butene			-0.75
butane			-0.27
C_{4+}			-2.27
CH_4			-9.28
CO_2			-8.79
Wastewater			-5.76
Electricity	$MWh\ t_e^{-1}$	230.84	-15.91
H_2 Heat			
H_2 Feed		94.80	
CapEx	M£	36194.55	1612.80

S. 6.7 HTeCO + S-eC_2H_4

Table S. 28: Detailed mass and energy balances of the HTeCO and S-eC_2H_4 processes.

Stream	Unit	Process	
		HTeCO	**S-eC_2H_4**
CO_2	$t\ t_e^{-1}$	4.35	
H_2O			3.32
CO		**-2.77**	**2.77**
O_2		-1.58	-2.95
Ethylene			**-1.00**
CO_2			-0.89
Wastewater			-2.04
Electricity	$MWh\ t_e^{-1}$	17.74	31.15
H_2 Heat			
CapEx	M£	2781.88	3759.55

S. 6.8 D-FT

Table S. 29: Detailed mass and energy balances of the D-FT processes.

Stream	Unit	D-FT
CO_2	$t\ t_e^{-1}$	18.27
Air		32.65
H_2O		
O_2		
Ethylene		**-1.00**
Ethane		-0.26
Propylene		-1.36
Propane		-0.29
butene		-1.30
butane		-0.25
C_{4+}		-0.49
CO_2		*Not determined due to lack of data*
Wastewater		*Not determined due to lack of data*
Electricity	$MWh\ t_e^{-1}$	0.07
H_2 Heat		4.24
H_2 Feed		135.99
CapEx	M£	5715.17

S. 6.9 D-eC_2H_4

Table S. 30: Detailed mass and energy balances of the D-eC_2H_4 process.

Stream	Unit	D-eC_2H_4
CO_2	$t\ t_e^{-1}$	3.73
Air		
H_2O		5.84
O_2		-5.19
Ethylene		**-1.00**
Ethane		
Propylene		
Propane		
butene		
butane		
C_{4+}		
CO_2		-0.16
Wastewater		-2.75
Electricity	$MWh\ t_e^{-1}$	45.85
H_2 Heat		4.58
H_2 Feed		
CapEx	M£	7535.06

References

1. Olympios A V, Mersch M, Sapin P, Pantaleo AM, Markides CN. *Library of price and performance data of domestic and commercial technologies for low-carbon energy systems*. 2021. https://doi.org/10.5281/ZENODO.4692649.

2. Pérez-Fortes M, Schöneberger JC, Boulamanti A, Tzimas E. Methanol synthesis using captured CO2 as raw material: Techno-economic and environmental assessment. *Applied Energy*. 2016;161: 718–732. https://doi.org/10.1016/J.APENERGY.2015.07.067.

3. Chen YH, Hsieh W, Chang H, Ho CD. Design and economic analysis of industrial-scale methanol-to-olefins plants. *Journal of the Taiwan Institute of Chemical Engineers*. 2022;130: 103893. https://doi.org/10.1016/J.JTICE.2021.05.040.

4. Chen YH, Hsieh W, Chang H, Ho CD. Design and economic analysis of industrial-scale methanol-to-olefins plants. *Journal of the Taiwan Institute of Chemical Engineers*. 2022;130: 103893. https://doi.org/10.1016/J.JTICE.2021.05.040.

5. Towler G, Sinnot R. *Chemical Engineering Design - Principles, Practice and Economics of Plant and Process Design*.. 3rd ed. Elsevier; 2022.

6. Jenkins S. *Chemical engineering plant cost index: 2019 annual value*. Chemical Engineering Online.

7. Chauvy R, Verdonck D, Dubois L, Thomas D, De Weireld G. Techno-economic feasibility and sustainability of an integrated carbon capture and conversion process to synthetic natural gas. *Journal of CO2 Utilization*. 2021;47: 1–10. https://doi.org/10.1016/j.jcou.2021.101488.

8. Spallina V, Velarde IC, Jimenez JAM, Godini HR, Gallucci F, Van Sint Annaland M. Techno-economic assessment of different routes for olefins production through the oxidative coupling of methane (OCM): Advances in benchmark technologies. *Energy Conversion and Management*. 2017;154: 244–261. https://doi.org/10.1016/J.ENCONMAN.2017.10.061.

9. Liu Y, Kamata H, Ohara H, Izumi Y, Ong DSW, Chang J, et al. Low-Olefin Production Process Based on Fischer-Tropsch Synthesis: Process Synthesis, Optimization, and Techno-Economic Analysis. *Industrial and Engineering Chemistry Research*. 2020;59(18): 8728–8739. https://doi.org/10.1021/ACS.IECR.0C00542/SUPPL_FILE/IE0C00542_SI_001.PDF.

10. Do TN, Kim J. Green C2-C4 hydrocarbon production through direct CO2 hydrogenation with renewable hydrogen: Process development and techno-economic analysis. *Energy Conversion and Management*. 2020;214: 112866. https://doi.org/10.1016/J.ENCONMAN.2020.112866.

11. Gazzani M, Turi DM, Manzolini G. Techno-economic assessment of hydrogen selective membranes for CO2 capture in integrated gasification combined cycle. *International Journal of Greenhouse Gas Control*. 2014;20: 293–309. https://doi.org/10.1016/j.ijggc.2013.11.006.

12. Wang C, Liu Y, Ren H, Guan Q, Chou S, Li W. Diminishing the Uncoordinated N Species in Co-N-C Catalysts toward Highly Efficient Electrochemical CO2 Reduction. *ACS Catalysis*. 2022;12(4): 2513–2521. https://doi.org/10.1021/acscatal.1c05029.

13. Zhang XY, Li WJ, Wu XF, Liu YW, Chen J, Zhu M, et al. Selective methane electrosynthesis enabled by a hydrophobic carbon coated copper core-shell architecture. *Energy and Environmental Science*. 2022;15(1): 234–243. https://doi.org/10.1039/d1ee01493e.

14. Ji Y, Yang C, Qian L, Zhang L, Zheng G. Promoting electrocatalytic carbon monoxide reduction to ethylene on copper-polypyrrole interface. *Journal of Colloid and Interface Science*. 2021;600: 847–853. https://doi.org/10.1016/j.jcis.2021.05.057.

15. Dinh CT, Burdyny T, Kibria MG, Seifitokaldani A, Gabardo CM, Pelayo García De Arquer F, et al. CO 2 electroreduction to ethylene via hydroxide-mediated copper catalysis at an abrupt interface. *Science*. 2018;360: 783–787. https://www.science.org

16. Hansen KU, Cherniack LH, Jiao F. Voltage Loss Diagnosis in CO_2 Electrolyzers Using Five-Electrode Technique. *ACS Energy Letters*. 2022;7(12): 4504–4511. https://doi.org/10.1021/acsenergylett.2c02096.

17. Qiu YL, Zhong HX, Zhang TT, Xu W Bin, Li XF, Zhang HM. Copper Electrode Fabricated via Pulse Electrodeposition: Toward High Methane Selectivity and Activity for CO2 Electroreduction. *ACS Catalysis*. 2017;7(9): 6302–6310. https://doi.org/10.1021/acscatal.7b00571.

18. Millet P, Ngameni R, Grigoriev S a., Mbemba N, Brisset F, Ranjbari A, et al. PEM Water Electrolyzers: From Electrocatalysis to Stack Development. *Int. J. Hydrogen Energy*. 2010;35: 5043.

19. Endrődi B, Kecsenovity E, Samu A, Darvas F, Jones R V, Török V, et al. Multilayer Electrolyzer Stack Converts Carbon Dioxide to Gas Products at High Pressure with High Efficiency. *ACS Energy Letters*. 2019;4(7): 1770–1777. https://doi.org/10.1021/acsenergylett.9b01142.

20. Gawel A, Jaster T, Siegmund D, Holzmann J, Lohmann H, Klemm E, et al. Electrochemical CO2 reduction - The macroscopic world of electrode design, reactor concepts & economic aspects. *iScience*. 2022;25(4): 104011. https://doi.org/https://doi.org/10.1016/j.isci.2022.104011.

21. Miller HA, Bouzek K, Hnat J, Loos S, Bernäcker CI, Weißgärber T, et al. Green hydrogen from anion exchange membrane water electrolysis: a review of recent developments in critical materials and operating conditions. *Sustainable Energy & Fuels*. 2020;4(5): 2114–2133. https://doi.org/10.1039/C9SE01240K.

22. Adnan MA, Kibria MG. Comparative techno-economic and life-cycle assessment of power-to-methanol synthesis pathways. *Applied Energy*. 2020;278: 1–12. https://doi.org/10.1016/j.apenergy.2020.115614.

23. Salvatore DA, Gabardo CM, Reyes A, O'Brien CP, Holdcroft S, Pintauro P, et al. Designing anion exchange membranes for CO2 electrolysers. *Nature Energy*. 2021;6(4): 339–348. https://doi.org/10.1038/s41560-020-00761-x.

24. Kaczur JJ, Yang H, Liu Z, Sajjad SD, Masel RI. Carbon Dioxide and Water Electrolysis Using New Alkaline Stable Anion Membranes. *Front. Chem.* 2018;6: 263.

25. Endrődi B, Kecsenovity E, Samu A, Halmágyi T, Rojas-Carbonell S, Wang L, et al. High carbonate ion conductance of a robust PiperION membrane allows industrial current density and conversion in a zero-gap carbon dioxide electrolyzer cell. *Energy & Environmental Science*. 2020;13(11): 4098–4105. https://doi.org/10.1039/D0EE02589E.

26. Wakerley D, Lamaison S, Wicks J, Clemens A, Feaster J, Corral D, et al. Gas diffusion electrodes, reactor designs and key metrics of low-temperature CO2 electrolysers. *Nature Energy*. 2022;7(2): 130–143. https://doi.org/10.1038/s41560-021-00973-9.

27. Rabinowitz JA, Kanan MW. *The future of low-temperature carbon dioxide electrolysis depends on solving one basic problem*. Nature Communications. 2020. https://doi.org/10.1038/s41467-020-19135-8.

28. International Renewable Energy Agency T. *GREEN HYDROGEN COST REDUCTION SCALING UP ELECTROLYSERS TO MEET THE 1.5°C CLIMATE GOAL H 2 O 2*. 2020. www.irena.org/publications

29. Moreno-Gonzalez M, Berger A, Borsboom-Hanson T, Mérida W. Carbon-neutral fuels and chemicals: Economic analysis of renewable syngas pathways via CO2 electrolysis. *Energy Conversion and Management*. 2021;244: 1–17. https://doi.org/10.1016/j.enconman.2021.114452.

30. Mayyas A, Ruth M, Pivovar B, Bender G, Wipke K. *Manufacturing Cost Analysis for Proton Exchange Membrane Water Electrolyzers*. 2019. https://www.nrel.gov/docs/fy10osti/72740.pdf.

31. London Metal Exchange - Prices for Non-ferrous and Minor Metals. *Armen Press News Wire*. 2019.

32. Gavin Towler, Ray Sinnot. *Chemical Engineering Design - Principles, Practice and Economics of Plant and Process Design*.. 3rd ed. Elsevier; 2022.

33. Jones DA. *Technoeconomic Evaluation of MEA versus Mixed Amines and a Catalyst System for CO2 Removal at Near-Commercial Scale at Duke Energy Gibson 3 Plant and Duke Energy Buck NGCC Plant*. 2018 Jan.

34. Bachman JE, Reed DA, Kapelewski MT, Chachra G, Jonnavittula D, Radaelli G, et al. Enabling alternative ethylene production through its selective adsorption in the metal–organic framework Mn $_2$ (*m* -dobdc). *Energy & Environmental Science*. 2018;11(9): 2423–2431. https://doi.org/10.1039/C8EE01332B.

35. Ramdin M, De Mot B, Morrison ART, Breugelmans T, Van Den Broeke LJP, Trusler JPM, et al. Electroreduction of CO2/CO to C2Products: Process Modeling, Downstream Separation, System Integration, and Economic Analysis. *Industrial and Engineering Chemistry Research*. 2021;60(49): 17862–17880. https://doi.org/10.1021/acs.iecr.1c03592.

36. Matthew James Labuda, Timothy Christopher Golden, Roger Dean Whitley, Craig E. Steigerwalt. *Performance stability in rapid cycle pressure swing adsorption systems*. United States; 2006.

37. Buchner GA, Zimmermann AW, Hohgräve AE, Schomäcker R. Techno-economic Assessment Framework for the Chemical Industry—Based on Technology Readiness Levels. *Industrial & Engineering Chemistry Research*. 2018;57(25): 8502–8517. https://doi.org/10.1021/acs.iecr.8b01248.

38. Seider WD, Lewin DR, Seader J. D., Widagdo S, Gani R., Ng KM. *Product and Process Design Principles - Synthesis, Analysis, and Evaluation*.. 4th ed. New York: John Wiley & Sons, Inc.; 2017.

39. Subraveti SG, Roussanaly S, Anantharaman R, Riboldi L, Rajendran A. Techno-economic assessment of optimised vacuum swing adsorption for post-combustion CO2 capture from steam-methane reformer flue gas. *Separation and Purification Technology*. 2021;256: 117832–117852. https://doi.org/10.1016/j.seppur.2020.117832.

40. Haldor Topsoe. *Carbon Monoxide*. https://www.topsoe.com/processes/carbon-monoxide.

41. Jakobsson NB, Pedersen CF, Hansen JB. *PROCESS FOR PRODUCING CO FROM CO2 IN A SOLID OXIDE ELECTROLYSIS CELL*. United States; US10494728B2, 2019.

42. Glenk G, Holler P, Reichelstein S. Advances in power-to-gas technologies: cost and conversion efficiency. *Energy & Environmental Science*. 2023;16(12): 6058–6070. https://doi.org/10.1039/D3EE01208E.

43. James BD, Prosser JH. *HTE Stack Manufacturing Cost Analysis*. 2022.

44. Peterson D, Miller E. *Hydrogen Production Cost from Solid Oxide Electrolysis*. 2016.

45. Topsoe A/S. *Topsoe PtX: Bridging the gap* . 2021.

46. Environment Agency. *Wilton Olefins Installation Variation and consolidation application number EPR/BS3590IE/V014 1 Notice of variation and consolidation with introductory note Variation application number Permit number*. 2016.

47. Sabic UK. *Teesside - Wilton Site*. https://www.sabic-teesside.co.uk/en/teesside-site/wilton-site [Accessed 2nd February 2022].

48. Brelsford R. *ExxonMobil plans upgrades at UK ethylene plant | Oil & Gas Journal*. https://www.ogj.com/refining-processing/petrochemicals/article/14040637/exxonmobil-plans-upgrades-at-uk-ethylene-plant [Accessed 2nd February 2022].

49. Ineos. *Products | INEOS Olefins & Polymers Europe*. https://www.ineos.com/businesses/ineos-olefins-polymers-europe/products/ [Accessed 2nd February 2022].

50. Short W, Packey DJ, Holt T. *A manual for the economic evaluation of energy efficiency and renewable energy technologies*. 1995.